POLITECNICO DI TORINO
Repository ISTITUZIONALE

Mesomechanical modeling of debonding failures in FRP-strengthened structures

Publisher copyright

(Article begins on next page)

04 August 2020

Mesomechanical modeling of debonding failures in FRP-strengthened structures

Laura De Lorenzis[1], Viviana Palmieri[2], and Giorgio Zavarise[3]

[1] Technische Universität Braunschweig, Germany, l.delorenzis@tu-braunschweig.de
[2] University of Salento, Lecce, Italy, viviana.palmieri@unisalento.it
[3] University of Salento, Lecce, Italy, giorgio.zavarise@unisalento.it

ABSTRACT: Debonding mechanisms in FRP-strengthened structures have been the subject of numerous investigations. Most of the modeling studies conducted thus far are based on the assumption of macroscopic relationships between local interfacial stresses and local relative displacements between FRP and substrate. Such laws are calibrated experimentally and incorporated in structural models with the purpose of determining macroscopic quantities of design interest. This approach presents a number of limitations, as macroscopic interfacial laws spatially homogenize complex damage and failure processes taking place at the lower scales. This paper proposes an alternative approach to the problem of FRP debonding, based on a mesomechanical analysis including explicit description of the interfacial geometry, and illustrates the first steps taken by the authors in this direction. The final goal is to be able to design and optimize the macroscopic interfacial behavior by tailoring the features at the lower scale. Also, a deeper understanding of mixed-mode interfacial failures is aimed at. The paper illustrates the basic idea, the main details about the current implementation, and preliminary numerical results.

1 INTRODUCTION

Debonding mechanisms often control failure of FRP-strengthened structures. As a result, they have been addressed in a vast amount of research studies. Most of the modeling efforts conducted thus far are based on the assumption of macroscopic relationships relating the local interfacial shear and normal stresses to the local relative displacements between FRP and substrate. This assumption stems from the field of non-linear fracture mechanics, and in particular from the so called cohesive-zone (CZ) modeling approach (Hillerborg et al. 1976).

CZ models for interfaces between FRP and substrates of different materials have been calibrated experimentally and incorporated in several structural models to determine macroscopic quantities of design interest. Hereafter, explicit reference will be made to concrete substrates.

Despite its wide employment and reasonable success especially in single-mode loading cases, this approach presents a number of shortcomings:

a) CZ models based on macro-scale phenomenology spatially homogenize all effects that occur at the interface. Hence, the calibrated parameters of a macroscale CZ law may vary significantly as the experimental setup changes, and a law calibrated for a certain geometry and test setup is not necessarily accurate to simulate the same interface for different loading conditions or system geometries (e.g. in the strengthened structure);
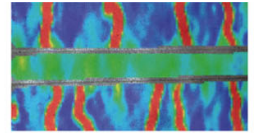
b) macroscopic CZ models depend on material properties and need to be re-obtained anytime a different material system is used. The experimental observations indicate as mode-II debonding typically occurs by formation of a cracking pattern a few millimeters from the bond line, whereas mode-I or mixed-mode debonding may involve a larger substrate thickness. The actual distribution of aggregates, the properties of the mortar, the presence of a superficial primer- and resin-modified region affected by factors such as porosity and primer/resin viscosity cannot be directly reflected in a macroscopic law;

c) mixed-mode CZ laws suitable for the FRP-concrete interface are still an open issue. The models available for different material systems are not necessarily suitable for this case, due to possibly different microscopic damage mechanisms.

A solution to each of these issues can be found by accounting explicitly for the processes occurring at the lower scales, and transferring these informations to the macroscale in a consistent manner. This is the idea underlying multiscale approaches, which are currently applied in several fields of science and engineering. This paper describes the first steps taken by the authors towards the multiscale modeling of debonding in FRP-concrete joints. The focus is on the mesoscale, where the coarser aggregates are explicitly described and the finer aggregates are incorporated in the mortar behavior. A multiscale transition is devised to derive macroscopic laws based on mesostructural details. This approach can shed light on the role played by the mesoscale parameters and lead to tailoring and optimization of the lower-scale features to achieve a desired macroscale response.

2 MESOMECHANICAL MODEL FOR CONCRETE

2.1 Previous work

Several mesomechanical models have been developed to study the damage and failure mechanisms of concrete and other quasi-brittle heterogeneous materials. Early models were either based on idealized mesostructures (random particle model, Bazant et al. 1990, framework model, Schorn & Rode 1991, and lattice model, Schlangen & van Mier 1992), or on a realistic description of the aggregate geometry (Wittmann et al. 1984, De Schutter and Taerwe 1993). More recent models are mostly based on the latter approach, and typically consider concrete as a three-phase composite including mortar, coarse aggregate and the interfacial transition zone (Wang et al. 1999, Teng et al. 2004, Zhu et al. 2004, Häfner et al. 2006, Snozzi et al. 2011). These models mainly differ from each other in the representation of the geometry, as well as in the material models used for the single phases. The method for the geometry description ranges from hand drawing (Zhu et al. 2004) to Voronoi tessellation (Snozzi et al. 2011) to ad-hoc elaborated procedures incorporating random variables (Wang et al. 1999). The material models include rotating crack, damage and CZ approaches. In spite of the differences, all these models share the objective to derive the macroscopic mechanical response of concrete from the detailed consideration of the meso-level geometry and material behavior.

The vast majority of the previous studies considered a 2D geometry, which is a rather crude assumption but maintains the computational effort within reasonable limits. Wriggers and Moftah (2006) presented a 3D approach with aggregates of spherical shapes. In this paper, we limit ourselves to a 2D geometry, however the extension to the 3D regime for angular aggregates is currently underway.

2.2   Definition of the geometry

2.2.1   Generalities

The concrete mesostructure is here intended as being constituted by the coarse aggregates and the cement paste with the finer aggregates embedded. Currently, the interfacial transition zone between coarse aggregates and paste is not taken into account but is planned to be included in future developments.

For the generation of the mesostructure, an important distinction is based on the shape of the coarse aggregates, which is generally taken as round or angular for gravel or crushed rock types, respectively. This paper considers concrete made with crushed rock aggregates, for which the procedure proposed by Wang et al. (1999) for the numerical generation of a random aggregate structure of angular shape is adopted. The main involved steps are summarized hereafter.

2.2.2   Grading curve and outline of the procedure

First of all, a suitable grading curve must be selected. This is given as a function $P(D)$, which represents the cumulative percentage of aggregate P passing through the sieve of aperture size D. The latter ranges between D_{min} and D_{max}, which coincide respectively with the minimum and maximum size of the coarse aggregate. Herein, the classical Fuller curve is adopted, i.e.

$$P = 100 \sqrt{\frac{D}{D_{max}}} \tag{1}$$

Once $P(D)$ is known, the area of aggregate contained within each grading segment $[D_i, D_{i+1}]$ can be computed as

$$A_{agg,i} = \frac{P(D_i) - P(D_{i-1})}{P(D_{max}) - P(D_{min})} A_{agg} \tag{2}$$

where A_{agg} is the total area of coarse aggregates, in turn equal to a desired fraction of the total concrete area, ranging for most concretes between 0.4 and 0.5.

The generation of the aggregate structure proceeds through a take-and-place process, which is conducted for each grading segment starting with the largest one and proceeding until the smallest. For the generic segment i, once its aggregate area $A_{agg,i}$ is computed with eq. (2), a number of particles of random shape and size are generated (take process) and placed (place process) into the area of the concrete specimen, until the area of aggregate left to be generated is insufficient for the creation of an additional particle within the same grading segment. When this condition is reached, the remaining aggregate area is added to the next grading segment and the procedure continues for this segment.

2.2.3   The take process

In the take process, the aggregate particles are generated as randomly shaped polygons, with size (i.e. width) dictated by the current grading segment and elongation (i.e. length to width ratio) prescribed as a random variable uniformly distributed between two predetermined values λ_{min} and λ_{max}.

The shape of a polygon is completely defined by the number of sides n, and by the polar radii r_j and the polar angles θ_j of the n vertices. Following visual observations and in line with Wang et al. (1999), n is taken herein as a random integer variable uniformly distributed between 4 and 10. The polar radii r_j are also considered as uniformly distributed random variables in the range between r_{min} and r_{max}, whereas the polar angles are found by first computing the angles subtended by consecutive sides, $\phi_j = \theta_{j+1} - \theta_j$. The latter are taken as random variables,

uniformly distributed with an average value $2\pi/n$ and assumed to differ from this average by a maximum of $\delta 2\pi/n$, with a predetermined value of $\delta \leq 1$. The subtended angles obtained from the random procedure are normalized to ensure that their sum equals 2π, as follows

$$\widetilde{\phi}_j = \frac{2\pi}{\sum_k \phi_k} \phi_j \tag{3}$$

and the polar angles are subsequently evaluated as

$$\theta_j = \alpha + \sum_{k=1}^{j-1} \widetilde{\phi}_k \tag{4}$$

where α is a phase angle determining the orientation of the particle, also obtained from a random uniform distribution.

Each particle as it results from the random generation procedure features a size and an elongation that do not necessarily correspond to the desired values. As in Wang et al. (1999), the size is herein assumed to coincide with the width of the particle, and the latter is computed as the minimum width of a rectangle excribing the particle, which is consistent with the meaning of variable D as the aperture size of a sieve. Also, the elongation is obtained as the length to width ratio of the minimum-width rectangle. Once the actual width and elongation of the particle are computed, straightforward scalings can be implemented to bring them to the desired values.

2.2.4 The place process

Once a particle is generated, its positioning within the concrete specimen requires that the coordinates of a reference point and the orientation angle α be specified. These three quantities are also considered as random variables, whereby the first two vary within the area of the concrete specimen and the last one between 0 and 2π. Also, it is assumed that each particle is surrounded by a mortar layer of thickness γ times the particle size. The value of γ is assumed to vary between γ_{min} and γ_{max}.

2.3   Material modeling

In this work, the aggregates are considered linearly elastic, the cement matrix is modeled with the isotropic damage law by Mazars (Pijaudier-Cabot & Mazars 2001), and a perfect interface is assumed between these two phases in the current implementation. The main features of the damage model are briefly summarized as follows.

The isotropic damage model by Mazars adopts a single scalar damage variable d, ranging from 0 for the undamaged state to 1 for the fully damaged state. Thus the stress-strain relation reads

$$\varepsilon_{ij} = \frac{1+v_0}{E_0(1-d)} \sigma_{ij} - \frac{v_0}{E_0(1-d)} \sigma_{kk} \delta_{ij} \tag{5}$$

where E_0 and v_0 are respectively the elastic modulus and the Poisson's ratio of the undamaged material, σ_{ij} and ε_{ij} are the stress and strain components, and δ_{ij} is Kronecker's delta. The damage variable is evaluated from an appropriate combination of tension and compression damage, as follows

$$d = \alpha_t d_t + \alpha_c d_c \tag{6}$$

where d_t and d_c are the damage variables in tension and compression, respectively, combined through the weigthing coefficients α_t and α_c.

The weithing coefficients are obtained through the decomposition of the principal stress tensor into a positive and a negative part, and through the computation of the corresponding tensile and compressive strains (Pijaudier-Cabot & Mazars 2001). The damage variables in tension and compression evolve based on the following relationships

$$d_t = 1 - \frac{\kappa_0(1-A_t)}{\tilde{\varepsilon}} - \frac{A_t}{exp[B_t(\tilde{\varepsilon}-\kappa_0)]}; \; d_c = 1 - \frac{\kappa_0(1-A_c)}{\tilde{\varepsilon}} - \frac{A_c}{exp[B_c(\tilde{\varepsilon}-\kappa_0)]} \tag{7}$$

where the equivalent strain $\tilde{\varepsilon}$ is defined as

$$\tilde{\varepsilon} = \sqrt{\sum_{i=1}^{3}(\langle\varepsilon_i\rangle)^2} \tag{8}$$

In eq. (8), $\langle\cdot\rangle$ are the Macaulay brackets and ε_i are the principal strains. As can be inferred from eqs. (5) and (7), this material model requires 7 parameters: E_0, ν_0, κ_0, A_t, B_t, A_c, B_c. Beside E_0 and ν_0 whose meaning is clear, κ_0 can be set as the strain at peak stress of the material under uniaxial tension, i.e.

$$\kappa_0 = \frac{f_t}{E_0} \tag{9}$$

where f_t is the material tensile strength.

In the present 2D implementation, plane stress conditions are assumed. Within a 2D approximation, plane stress conditions are believed to be more realistic as they correspond to simulating a concrete specimen of small thickness. In such a case it is reasonable that the aggregate geometry be constant across the thickness. Conversely, plane strain conditions imply a large out-of-plane thickness which contradicts the 2D nature of the aggregate geometry.

3   BENCHMARKING

3.1   Generalities

Before being used for modeling of the FRP-concrete interface, the mesomechanical concrete model described in the previous section was tested under simple loading conditions, including uniaxial tension and uniaxial compression. For ther latter tests, a square concrete specimen with 100 mm size was used, see Figure 1.

The geometry was created with the procedure outlined in Sect. 2.2, using the geometry parameters in Table 1. This geometry was then automatically meshed with triangular linear elements using the advancing front technique. Matching meshes for aggregate and mortar were obtained, with coincident nodes at the boundary due to the absence of interfacial elements in the current implementation.

Local damage models are well known to suffer from mesh sensitivity induced by strain localization. To circumvent this problem, non-local or gradient enhancements of the model are needed and are currently being pursued. For the heterogeneous concrete specimen as opposed to a homogeneous one, the size of the element has an upper bound equal to the minimum distance between aggregates. For consistency of the multiscale procedure, the lower bound should be set as the maximum characteristic length of the lower scale, e.g. the size of the small aggregates which are considered dispersed in the mortar.

3.2 First results

Table 1 summarizes the material parameters for the mortar and the aggregates. These parameters were calibrated by means of the uniaxial tension and uniaxial compression tests for a concrete of 30 MPa compressive strength containing 40% coarse aggregates. The corresponding stress-strain curves are illustrated in Figure 1.

Table 1. Geometry and material parameters.

D_{min} (mm)	D_{max} (mm)	A_{agg}(%)	δ	λ_{min}	λ_{max}	γ_{min}	γ_{max}
4.0	10.0	40	0.7	1.0	3.0	0.005	0.15

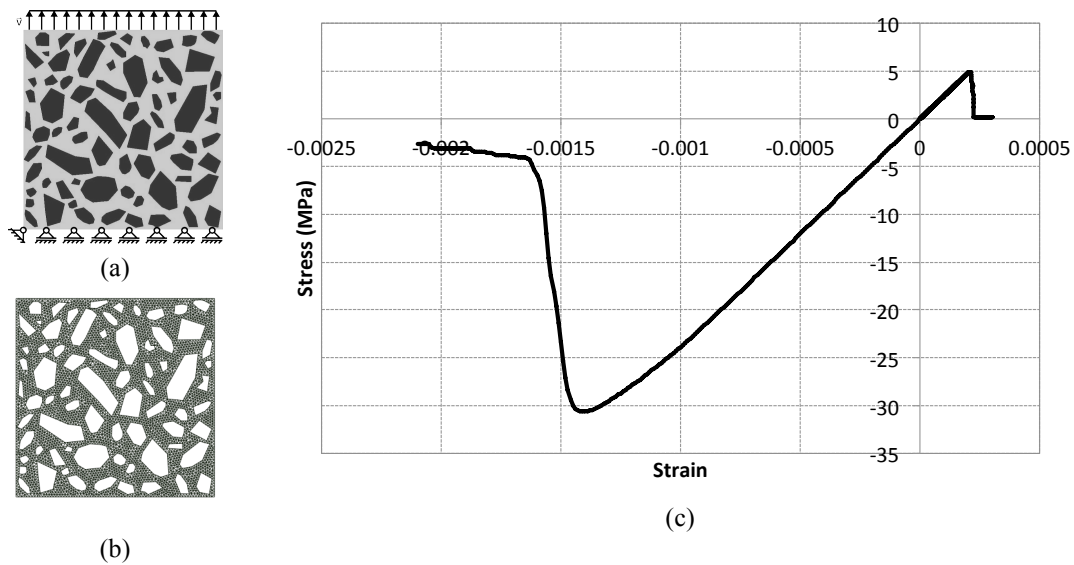| Mortar						Aggregate	
E_0 (MPa)	ν_0	κ_0	A_t	B_t	A_c	B_c	E_{agg} (MPa)	ν_{agg}
16000	0.2	0.0005	1.0	10000	1.5	500	50000	0.2

(a)

(b)

(c)

Figure 1. Geometry (a) and mesh (b) of a numerical specimen subjected to tensile testing. (c) Stress-strain curves in uniaxial tension (positive values) and compression (negative values) for the model parameters in Table 1.

4 MULTISCALE APPROACH FOR THE FRP-CONCRETE INTERFACE

4.1 Formulation

Herein, a multiscale cohesive framework is set up for the FRP-concrete interface to relate damage and failure processes taking place at the mesoscale to a macroscopic CZ model. This framework follows the approach proposed by Matouš et al. (2008). The macro- and mesoscales are linked using an energy-based computational homogenization procedure, which relies on an implementation of Hill's stationarity condition. This scheme does not place any restrictions on

the stiffness of individual constituents. Heterogeneous interfaces with randomly distributed inclusions of an arbitrary shape and size can be investigated. Moreover, a computationally attractive coupling between scales is obtained.

The starting point of the procedure is the definition of a representative volume element (RVE). In the present study, local periodicity of the interface is assumed, which simplifies the choice of the RVE by eliminating the need for sample enlargement and ensemble averaging. The study of a statistically representative RVE for non-periodic interfaces is one of the extensions to be pursued in future work. Moreover, the RVE considered hereafter does not consider the influence of the primer and resin layers but only includes the superficial layer of concrete underneath the FRP sheet. In order for a detailed and realistic geometry to be described, experimental quantitative observations are needed.

A micromechanical test setup is developed on which computational homogenization is carried out. In order for the assumption of scale separation to hold, thickness and width of the RVE must be suitably larger than the maximum aggregate size. Herein we considered a thickness of 20 mm and a width of 80 mm. The RVE is subjected to periodic boundary conditions on the lateral sides, due to the assumed local periodicity. The lower edge is considered fixed, whereas the upper edge is subjected to a monotonically increasing uniform displacement. Depending upon the direction of this applied displacement, pure mode-I, mode-II or mixed-mode conditions with a desired mode mixity can be obtained. The macroscopic tractions in the two directions are obtained as the summation of the reaction forces in the same directions at all the nodes of the upper edge of the RVE. The first results presented as follows were obtained in mode-I conditions, see Figure 2.

4.2 First results

Figure 2 shows the distribution of the damage variable d in the RVE under pure mode-I loading at failure. Figure 2a refers to the specimen directly obtained by the geometry procedure illustrated earlier. As aggregates are automatically generated at a minimum distance from the boundary of the domain, a superficial layer of mortar is produced. As a result, failure is localized in this layer. In real applications, it is common practice to remove the superficial mortar layer and expose the underlying aggregates e.g. through sandblasting. If such a procedure is reflected by removing the superficial layer of elements in the finite element model (Figure 2b), the damage distribution involves a thicker material layer and the mode-I strength and fracture energy of the interface are consequently increased (Figure 2c).
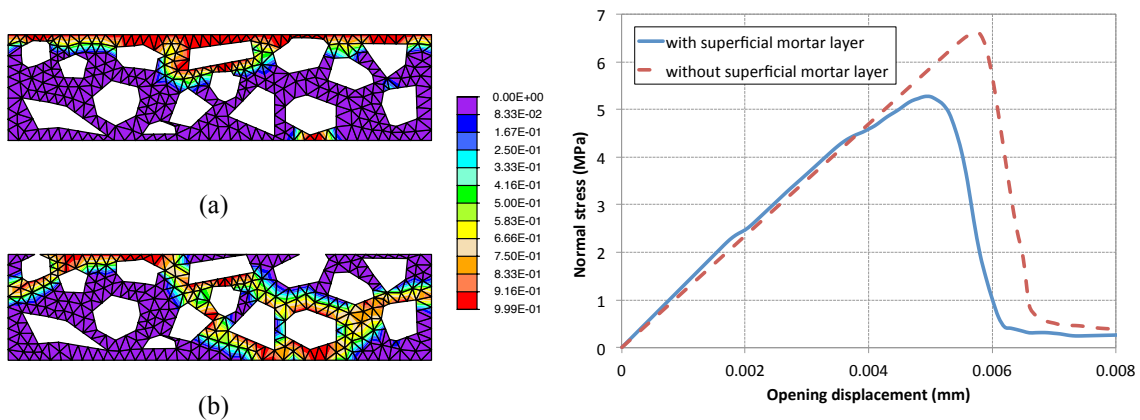

Figure 2. Damage variable distribution within the RVE at failure under mode-I loading with (a) and without (b) superficial layer of mortar. (c) Macroscopic mode-I CZ model.

5   CONCLUSIONS

This paper proposes a multiscale approach through which cohesive zone laws for the FRP-concrete interface under variable mode mixity can be derived through a detailed examination of the mesoscale geometry and a suitable constitutive modeling of the constituent materials. The first results show the capability and flexibility of the approach to interpret changes in the mesoscale geometry and translate these into macroscopically different results. Further research is currently ongoing including the improvement of the model (non-local or gradient mortar constitutive description, incorporation of the interfacial transition zone), the examination of the representativity of the numerical sample (in the periodic as well as non-periodic cases), the analysis of the role of the aggregate shape, size and distribution on the macroscopic results, the investigation of mixed-mode effects, the extension to more realistic mesoscale geometries including primer and resin materials and concrete porosity, and the extension to the 3D setting.

6   ACKNOWLEDGMENTS

7   REFERENCES

Bažant, ZP, Tabbara, MR, Kazemi, MT, and Pijaudier-Cabot, G. 1990. Random particle model for fracture of aggregate or fiber composites. *Journal of Engineering Mechanics*, ASCE, 116(8): 1686–1705.

De Schutter, G, and Taerwe, L. 1993. Random particle model for concrete based on Delaunay triangulation. *Materials and Structures*, 26(156): 67-73.

Häfner, S, Eckardt, S, Luther, T., and Könke, C. 2006. Mesoscale modeling of concrete: Geometry and numerics. *Computers and Structures*, 84: 450–461.

Hillberborg, A, Modeer, M, and Petersson, PE. 1976. Analysis of crack formation and crack growth in concrete by means of fracture mechanics and finite elements. *Cement and Concrete Research*, 6: 773–782.

Matouš, K, Kulkarni, MG, and Geubelle, PH. 2008. Multiscale cohesive failure modeling of heterogeneous adhesives. *Journal of the Mechanics and Physics of Solids*, 56: 1511–1533

Pijaudier-Cabot, G, and Mazars, J. 2001. Damage models for concrete, in: *Handbook of materials behavior models*, J. Lemaitre (ed.) Chapter 6 - Damage models, Academic Press, New York, 500-513.

Schlangen, E, and van Mier, JGM. 1992. Simple lattice model for numerical simulation of fracture of concrete materials and structures. *Materials and Structures*, 25(153): 534- 542.

Schorn, H, and Rode, U. 1991. Numerical simulation of crack propagation from microcraking to fracture. *Cement and Concrete Composites*, 13(2): 87-94.

Snozzi, L, Caballero, A, and Molinari, JF. 2011. Influence of the meso-structure in dynamic fracture simulation of concrete under tensile loading. *Cement and Concrete Research*, 41(11): 1130-1142.

Teng, JG, Zhu, WC, and Tang, CA. 2004. Mesomechanical model for concrete - Part II: Applications. *Magazine of Concrete Research*, 56(6): 331–345.

Wang, ZM, Kwan, AKH, and Chan, HC. 1999. Mesoscopic study of concrete I: generation of random aggregate structure and finite element mesh. *Computers and Structures*, 70: 533-544.

Wittmann, FH, Roelfstra, PE, and Sadouki, H. 1984. Simulation and Analysis of Composite Structures. *Materials Science and Engineering*, 68: 239-48.

Wriggers, P, and Moftah, SO. 2006. Mesoscale models for concrete: homogenisation and damage behaviour. *Finite Elements in Analysis and Design*, 42: 623 – 636.

Zhu, WC, Teng, JG, and Tang, CA. 2004. Mesomechanical model for concrete - Part I: Model Development. *Magazine of Concrete Research*, 56(6): 313-330.